

Special Collection

Effect of Ectoine on the Conformation and Hybridization of dsDNA in Monolayer Films: A Spectroelectrochemical Study

 Julia Wittmar,^[a, c] Corina Ohle,^[b, d] Jörg Kunte,^[b] and Izabella Brand*^[a]

Lack of long-time stability of dsDNA-based supramolecular assemblies is an important issue that hinders their applications. In this work, 20 base pairs long dsDNA fragments [(dCdG)₂₀-65%] composed of 65% dCdG and 35% dAdT nucleotides were tethered via a thiol to the surface of a gold electrode. The self-assembled (dCdG)₂₀-65% monolayer was immersed in solutions containing ectoine, a compatible solute. Electrochemical results showed that these monolayers were stable for one month. In situ IR spectroscopy indicated that ectoine interacts weakly with the phosphate-ribose backbone, dehydrating the

phosphate groups and stabilizing the A-DNA conformation. This structural reorganization led to a reorientation of nucleic acid base pairs and a local disruption of the double-helix structure. However, the conformation and orientation of the dsDNA fragment was stable in the $-0.4 < E < 0.3$ potential range. As a direct interaction between ectoine and dsDNA, the enzymatic reaction of exonuclease VII hydrolyzing the ester phosphate bond in ssDNA, was blocked. We show that the addition of a compatible solute to the electrolyte solution stabilized the dsDNA structure despite structural rearrangements.

1. Introduction

Research on biosensors involves interdisciplinary and complementary approaches aiming at the construction of selective bioanalytical devices that are composed of assembled biological recognition molecules. Future application fields of DNA-based sensors may be: The diagnostics of genetic diseases, detection of infectious agents, development of new classes of drugs, differentiation and recognition of genetic material, food safety or environment monitoring.^[1] The *modus operandi* of DNA-biosensors is linked either with the recognition of the hybridization state of DNA molecules or with the recognition of base mismatches, mutations, and lesions in dsDNA.^[1a] In general, the development of DNA-based sensing devices requires the immobilization of biomacromolecules on solid surfaces, with the aim of the formation or disruption of the

DNA double helix.^[1b] The selection of a detection method that distinguishes between properties of the double- (dsDNA) and single strand DNA (ssDNA) is the next critical step of sensor development. Electrochemical responses of dsDNA and ssDNA differ significantly, providing the foundation for the development of electrochemical DNA-biosensors.^[1a,2]


Following this, electrodes are required as supports for the immobilization of DNA, which includes either a physical adsorption^[1a] or a chemisorption.^[3] The chemical nature of the electrode material and the modification procedure influence the electrochemical properties of the adsorbed DNA molecules.^[1a,2b,c,4] An amperometric response is often used for the construction of electrochemical DNA-biosensors.^[1a] However, chemisorption of DNA molecules via a thiol-linker, followed by backfilling of the uncovered surface with a short alkanethiol monolayer, prevents the direct adsorption of the DNA fragments onto the metal surface. In these self-assembled monolayers (SAMs), nucleic-acid bases show no redox activity.^[1a,3a] Therefore, the electrochemical detection relies on the electrochemical interfacial properties of the adsorbed molecules, such as the film capacitance or potential of helix disruption.^[1a,5] To gain redox activity, redox labels that are able to intercalate into the dsDNA structure are used.^[2b,4] The electric potentials have a large impact on the stability, orientation, and hybridization state of the adsorbed dsDNA fragments.^[6] A net-positive charge of the electrode stabilizes, whereas a net-negative charge destabilizes the double helix DNA structure.^[1a,6b,7] In case of the commonly used 6–11 nm-long DNA duplexes (corresponding to 20–30 nucleotides), which are oriented upwards when attached to a metallic electrode, the impact of electric potentials depends on the distance from the electrode surface and composition of the DNA fragment. At distances of 5–8 nm (in most electrolyte solutions), the effect of electric fields is negligible.^[3b,6a,8] Despite this, negative potentials lead to the electrochemical destabilization of the double helix structure.^[6a,b,7,9]


[a] J. Wittmar, Dr. I. Brand
 Department of Chemistry
 University of Oldenburg
 26111 Oldenburg, Germany
 E-mail: izabella.brand@uni-oldenburg.de

[b] Dr. C. Ohle, Dr. J. Kunte
 Division Biodeterioration and Reference Organisms
 Bundesanstalt für Materialforschung und -prüfung BAM
 12205 Berlin, Germany

[c] J. Wittmar
 Institute of Cell Dynamics and Imaging
 Westfälische Wilhelms Universität Münster
 48149 Münster, Germany

[d] Dr. C. Ohle
 Deutsche Akkreditierungsstelle GmbH (DAkkS)
 Spittelmarkt 10, 10117 Berlin, Germany

 Supporting information for this article is available on the WWW under <https://doi.org/10.1002/celec.202100816>

 An invited contribution to the Marcin Opałto Festschrift.

© 2021 The Authors. ChemElectroChem published by Wiley-VCH GmbH. This is an open access article under the terms of the Creative Commons Attribution License, which permits use, distribution and reproduction in any medium, provided the original work is properly cited.

The results of electrochemically controlled atomic force microscopy (AFM),^[7] fluorescence spectroscopy,^[2d,3b] Raman spectroscopy,^[6b] or in situ polarization modulation infrared reflection absorption spectroscopy (PM IRRAS)^[6a] show that the packing and orientation of adsorbed dsDNA molecules in monolayers on gold surfaces depends on the electrode potential. At potentials more positive than the potential of zero charge (E_{pzc}), the helical axis is tilted toward the metal surface. The tilt angle varies between 25° and 70° to the surface normal.^[6a,7] In contrast, at negative potentials, the DNA helices align vertical to the surface, which is ascribed to electrostatic repulsion. Johnson et al. used a native negatively charged DNA and a neutral peptide nucleic acid (PNA) analogue to study the electrochemical melting of dsDNA.^[6b] They provided clear evidence that the potential-driven denaturation of DNA molecules adsorbed on a metal electrode surface is not caused by electrostatic repulsions, and instead suggested that it has to be connected with the composition of base pairs. Later, Kekedy-Nagy showed that the relative orientation and rotation of nucleic acid base pairs in dAdT and dCdG duplexes changes as a function of the electrode potential, which may be responsible for destabilization of the double strand structure at negative potentials.^[6a]

Nonetheless, *in operando* application of electrochemical DNA biosensors suffers from a poor understanding at the molecular level of the relationship between the structure of adsorbed DNA macromolecules, the potential drop at the electrode|electrolyte interface, the ionic strength of the electrolyte solution, and the sensor-recognizing properties. Even less is known about changes in the strength of hydrogen bonds between base pairs, the relative orientation of complementary bases, the hydration of the phosphate backbone, or the conformation of the sugar ring over time. These parameters affect the structure, conformation, and hybridization state of the DNA molecule and thus determine the functionality of a sensor. The molecular aspects of the aging process of dsDNA immobilized on solid supports are, to a large extent, unknown. However, it is well known that the SAMs of dsDNA are unstable over time, which is expressed in the disruption of hydrogen bonds between complementary base pairs, which eventually leads to dsDNA to ssDNA dehybridization.^[2a,6c,10]

Extremophilic microorganisms concentrate small, water-soluble organic molecules in their cytoplasm, called compatible solutes.^[11] Ectoine (1,4,5,6-tetrahydro-2-methyl-4-pyrimidinecarboxylic acid) is a widespread compatible solute (S1) in bacteria. Ectoine interacts strongly with surrounding water molecules, especially those present in the first hydration shell,^[12] affecting the hydration of biomolecules present in the cytoplasm. Compatible solutes destabilize various types of single- (ss) and double-stranded (ds) DNA,^[13] which is exhibited in a decrease in the melting temperature of dsDNA. The destabilization of the dsDNA structure was assigned to changes in the hydration state of the phosphate backbone of DNA due to the binding of water molecules by ectoine.^[14] Recent findings show that at the molecular level, ectoine interacts directly with the sugar-phosphate backbone of dsDNA.^[14a,15] This interaction has an effect on the hydration of the phosphate groups and the

respective orientation of the compatible base pairs, which leads to a transformation of the DNA helix from the B conformation to a less stable A conformation.^[14a] These structural changes result in a thermal destabilization of DNA, but do not lead to a dehybridization of the double helix structure. Interestingly, other studies report on protective properties of ectoine against dsDNA damage by UV light.^[13c,15] The effect of compatible solutes on the aging process of dsDNA is still not well understood, and is the subject of the current study.

Recognition of structural changes occurring in SAMs of dsDNA interacting with ectoine requires the use of non-invasive, label-free, and highly sensitive analytical techniques. Vibrational spectroscopy techniques are sensitive to the conformation and structure of organic molecules. They have frequently been applied to investigate the structure, conformation, and hybridization state of both dsDNA and ssDNA.^[16] The in situ determination of structural changes in DNA monolayers adsorbed on a solid surface is possible when reflection-based IRS techniques are applied.^[6a,14a]

In the current work, in situ PM IRRAS with electrochemical control was used to examine the interaction between ectoine and dsDNA in monolayer assemblies. The DNA fragment studied, (dCdG)₂₀-65 %, contained 20 base pairs and consisted of 65 % C and G and 35 % A and T. At $-0.4 < E < 0.4$ V vs Ag|AgCl, the conformation and orientation of the (dCdG)₂₀-65 % fragment was independent of the applied electric potentials. However, the interaction with ectoine led to significant changes in the (dCdG)₂₀-65 % monolayer over time. Dehydration of the phosphate groups led to a stabilization of the helical structure in the A conformation. This conformational change affected the relative position of compatible base pairs and the tilt of the helix axis in the (dCdG)₂₀-65 % fragment. Consequently, the double helix gained some orientational flexibility. However, as proven by enzymatic reaction studies with exonuclease VII, a local disruption of the hydrogen bonds between complementary base pairs did not lead to the dehybridization of the double helix to a single helix.

2. Results and Discussion

2.1. Electrochemical Characterization of the dsDNA Monolayer Interacting with Ectoine

After chemisorption of the thiolated (dCdG)₂₀-65 % fragments on the Au surface, the uncovered metal surface was backfilled with 6-mercapto-1-hexanol (further abbreviated as: SC₆OH). Since the SC₆OH was the main component of the SAM, electrochemical characterization of a pure SC₆OH film was first carried out. At $-0.4 < E < 0.4$ V vs Ag|AgCl RE, the capacitance of the SC₆OH monolayer in 10 mM PBS solution was $4.0 \pm 0.3 \mu\text{Fcm}^{-2}$, agreeing well with the capacitance measured by Steel.^[3a] The alkyl chain in the adsorbed thiol contains 6 methylene groups and the expected length of the chain is $d = 0.75$ nm. Alkyl chains in alkanethiol monolayers on Au are tilted by approximately 30° to the surface normal,^[17] thus, the expected monolayer thickness equaled 0.65 nm. The capaci-

tance of a defect-free monolayer (C) was calculated using equation 1,

$$C = \frac{\epsilon_0 \epsilon_r A}{d} \quad (1)$$

where ϵ_0 is the permeability of vacuum, ϵ_r is the dielectric constant of the monolayer (assumed to be 3), d is the thickness of the adsorbed film, and A is the surface area of the electrode. The calculated capacitance equaled $4.10 \mu\text{F cm}^{-2}$. This is in good agreement with our experimental values. Immersion of the SC_6OH monolayer in the PBS electrolyte solution containing 0.1 M ectoine led to a small increase in the film capacitance to $4.5 \pm 0.5 \mu\text{F cm}^{-2}$. Thus, ectoine molecules seemed to interact with the terminal hydroxide groups in the SC_6OH SAM. In PBS solution (pH 7.2), the SC_6OH monolayer desorbed from the Au surface at $E = -0.65 \text{ V}$.

Figure 1 shows the capacitance – potential plots of the $(\text{dCdG})_{20}\text{-65\%}$ SAM on the Au surface. Backfilling of the $(\text{dCdG})_{20}\text{-65\%}$ film with SC_6OH gave a compact monolayer with a capacitance of $\sim 4.5 \mu\text{F cm}^{-2}$ (Figure 1, black curve). Thus, the introduction of a short dsDNA fragment into the monolayer caused a slight increase in the capacitance, most likely as a consequence of an increase in the dielectric constant of the SAM.^[18] Over two weeks of storage of the monolayer in PBS solution, no significant changes in the capacitance of the dsDNA monolayer were observed. This result indicates that the monolayer structure and composition did not change over time. It agrees with our previous studies of dsDNA monolayers aging using X-ray photoelectron spectroscopy (XPS).^[14a]

In the electrolyte solution with ectoine, the capacitance of the $(\text{dCdG})_{20}\text{-65\%}$ SAM increased to approximately $5 \mu\text{F cm}^{-2}$ (Figure 1, dark red curve). In the first week, the capacitance changes were negligible, whereas in the second week, an accelerated increase in the capacitance was observed. Over

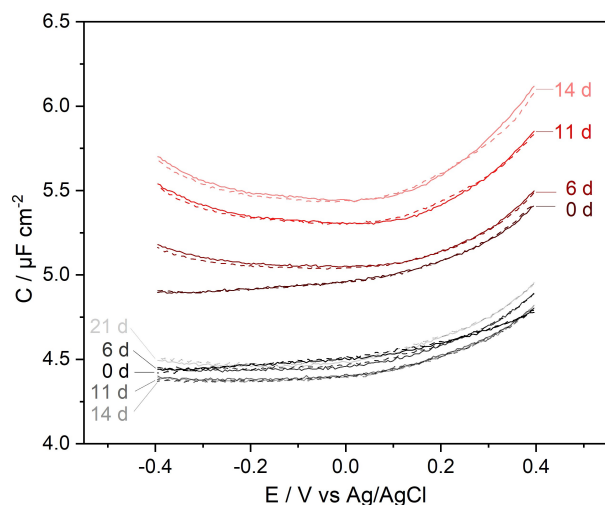


Figure 1. Capacitance – potential plots of the $(\text{dCdG})_{20}\text{-65\%}$ SAM on the Au surface in 10 mM PBS solution (black lines) and 10 mM PBS with 0.1 M ectoine solution (red lines) immersed in the corresponding electrolyte solution for different number of days as marked in the figure. Solid line – negative-going, and dashed line – positive-going potential scans.

14 days, the monolayer capacitance increased by $\sim 12\%$ and a weak capacitance minimum appeared at $E \approx 0.0 \text{ V}$ (Figure 1). The negative- and positive-going potential scans overlapped, which indicates a lack of potential-driven reorientations in the monolayer film. The dsDNA monolayer desorbed from the Au surface at $E = -0.61 \text{ V}$.

The electrochemical characteristics of the $(\text{dCdG})_{20}\text{-65\%}$ SAM could have been influenced by ectoine in the following way:

- A faster desorption of thiol molecules (predominantly DNA fragments) from the monolayer;
- Dehybridization of the dsDNA fragments;
- Changes in the orientation of the DNA helix with respect to the electrode surface, leading to some changes in the relative dielectric constant of the monolayer film.

Based on XPS results,^[14a] we were able to exclude the increase in the capacitance being caused by the desorption of thiol molecules from the Au surface. To elucidate the effect of ectoine and time on the hybridization, conformation, and orientation of the $(\text{dCdG})_{20}\text{-65\%}$ fragment in the monolayer, in situ PM IRRAS experiments with electrochemical control were carried out.

2.2. Conformation of the dsDNA Monolayers Interacting with Ectoine

Figure 2 shows in situ PM IRRAS spectra of the $(\text{dCdG})_{20}\text{-65\%}$ SAM in the glycosidic linkage, and phosphate frequencies region at $E = 0.0 \text{ V}$. This spectral region is sensitive to changes in the conformation and hydration of the dsDNA.^[16,19]

The electric potentials had no effect on the IR spectra of $(\text{dCdG})_{20}\text{-65\%}$ SAMs, indicating that neither hydration nor conformation of the dsDNA fragments changed as a function of

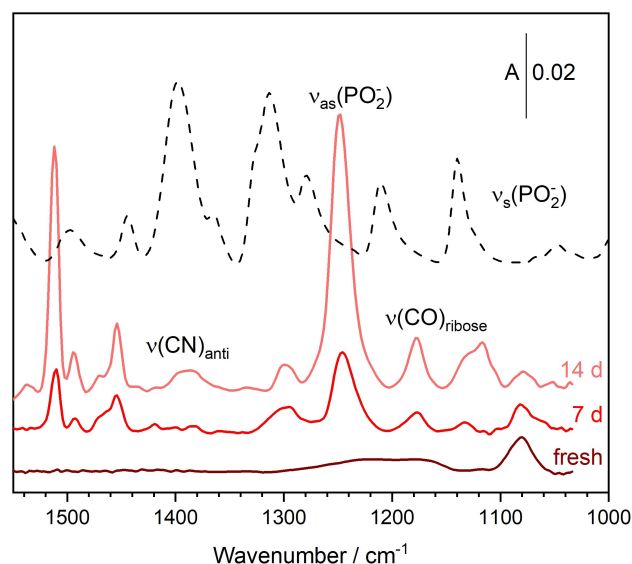


Figure 2. In situ PM IRRAS spectra in the $1550\text{--}1000 \text{ cm}^{-1}$ spectral region of a fresh $(\text{dCdG})_{20}\text{-65\%}$ SAM and 7-, 14-day-old $(\text{dCdG})_{20}\text{-65\%}$ SAM stored in 0.1 M ectoine in H_2O solution at $E = 0 \text{ V}$; Electrolyte solution 10 mM PBS in H_2O . Dashed black line: IR spectrum of ectoine in a KBr pellet.

the applied electric potential ($-0.4 \text{ V} < E < 0.3 \text{ V}$). However, in solutions containing ectoine, large spectral changes were observed. In the presence of ectoine, all absorption modes became better resolved. Their full width at half maximum (fwhm) decreased, while intensities of most IR absorption modes increased (Figure 2). Moreover, new IR absorption modes appeared in the in situ PM IRRAS spectra. To distinguish whether those new absorption bands were caused by the incorporation of ectoine into the (dCdG)₂₀₋₆₅% fragment, in situ spectra were compared with an IR transmission spectrum of ectoine in a KBr pellet (Figure 2, dashed line).

Overall, the overlap of ectoine and the (dCdG)₂₀₋₆₅% monolayer stored in 0.1 M ectoine solution spectra is poor, suggesting that ectoine binds weakly to the glycosidic linkage and the phosphate groups of dsDNA.

In the glycosidic linkage frequencies region, the largest spectral changes were observed at 1550–1450 cm^{-1} . In the 7-day-old (dCdG)₂₀₋₆₅% SAM new IR absorption modes appeared at 1515 cm^{-1} , 1495 cm^{-1} and 1450 cm^{-1} . Despite the fact that the modes at 1515 and 1495 cm^{-1} arose from the ring stretching and NH_2 deformation modes in nucleic-acid bases, they were not detected in the fresh (dCdG)₂₀₋₆₅% SAM. This is the consequence of the uniform packing of dsDNA fragments in the monolayer and will be discussed below. The weaker modes between 1470 and 1300 cm^{-1} are assigned to the CN stretching modes in the glycosidic linkage. The position of the $\nu(\text{CN})$ in the deoxyribose nucleic acid linkage depends on the *anti* or *syn* conformation of this linkage and thus A, B or Z conformation of the double helix.^[16c,20] Hydration of this molecular fragment additionally affects the frequency of this mode and may lead to its splitting, further complicating the structural analysis of this spectral region. The *anti* conformation of the CN linkage gives IR absorption modes at 1450, in 1425–1400 and 1370–1330 cm^{-1} .^[16c,e,19] The presence of the IR absorption modes around 1410–1380 and 1340 cm^{-1} indicate that upon interaction with ectoine, the (dCdG)₂₀₋₆₅% fragment exists in A conformation. A weak mode around 1300 cm^{-1} was specific to the dCdG base pair, which comprised 65% of the dsDNA fragment used in this study.^[6a]

The phosphate frequency region was strongly affected by the interaction of ectoine with (dCdG)₂₀₋₆₅%. In fact, the frequency of the $\nu_{\text{as}}(\text{PO}_2^-)$ mode is a spectral indicator of the DNA conformation.^[16b,21] In the fresh (dCdG)₂₀₋₆₅% monolayer, a broad (fwhm ca. 60 cm^{-1}) and weak $\nu_{\text{as}}(\text{PO}_2^-)$ mode was centered at 1222 cm^{-1} . On the high wavenumber side, it had a shoulder at 1240 cm^{-1} that was also assigned to the $\nu_{\text{as}}(\text{PO}_2^-)$. The existence of a broad phosphate stretching mode indicated that the hydration of the phosphate groups in the monolayer film varied between well-hydrated and poorly-hydrated. This spectral result indicates that the dsDNA exists in two helical conformations, namely in a well-hydrated B helix and a less-hydrated A helix. On the low wavenumber side, the $\nu_{\text{as}}(\text{PO}_2^-)$ mode overlapped with the $\nu(\text{CO})$ mode in the deoxyribose-phosphate backbone at 1179 cm^{-1} . This mode is characteristic for the helical A conformation of dsDNA. It agreed with our previous studies, which showed that in short CG-rich dsDNA, the A conformation is stabilized. Storage of the (dCdG)₂₀₋₆₅%

monolayer in ectoine solution led to a hypsochromic shift of the $\nu_{\text{as}}(\text{PO}_2^-)$ mode to 1246–1250 cm^{-1} and a decrease in fwhm to approximately 20 cm^{-1} , which indicates a lower hydration of the DNA in the monolayer. No significant spectral changes were observed in the frequency of the $\nu_{\text{s}}(\text{PO}_2^-)$ mode, which, indeed, is not strongly sensitive to hydration changes.^[16a,22] In summary, in the presence of ectoine the double helical to confirmation of the (dCdG)₂₀₋₆₅% fragments changed from a mixture of B- and A-DNA to exclusively A-DNA.

2.3. Orientation of the dsDNA Monolayers Interacting with Ectoine over Time

The effect of electric potentials on the stability and orientation of (dCdG)₂₀₋₆₅% SAMs on an Au surface was investigated by means of in situ PM IRRAS with electrochemical control. Figure 3 shows PM IRRAS spectra in the base stacking and glycosidic linkage frequency regions of the (dCdG)₂₀₋₆₅% SAMs aged in a solution containing 0.1 M ectoine. These experiments were carried out in D_2O to separate the IR absorption modes of the base pairs from the $\delta(\text{H}_2\text{O})$ in water. The isotopic substitution of H atoms in the amide groups by D led to a bathochromic shift

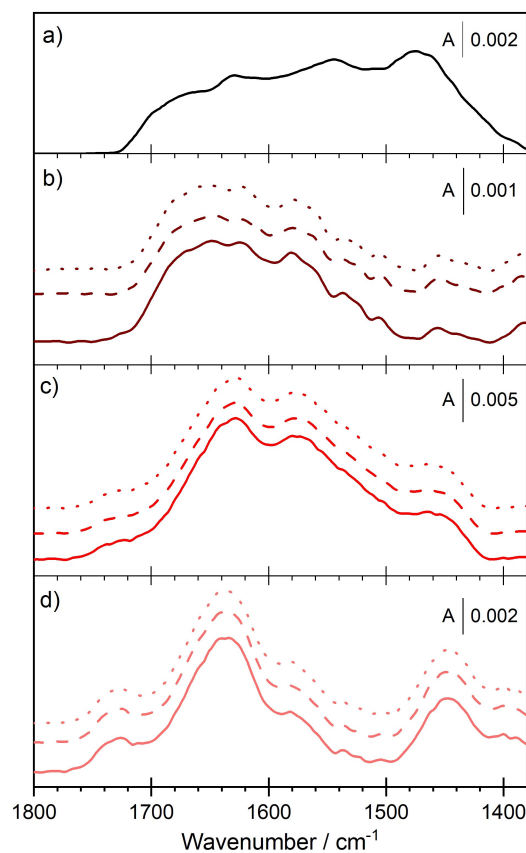


Figure 3. In situ PM IRRAS spectra in the 1800 cm^{-1} to 1400 cm^{-1} spectral region of a) randomly distributed (dCdG)₂₀₋₆₅% molecules in a monolayer film, b) 3-day-old (dCdG)₂₀₋₆₅% SAM, stored in 10 mM PBS in D_2O , c) 21- and d) 28-day-old (dCdG)₂₀₋₆₅% SAM stored 0.1 M ectoine solution in D_2O ; Electrolyte solution 10 mM PBS in D_2O at $E = -0.4$ (solid lines); $E = 0.0 \text{ V}$ (dashed lines) and $E = 0.3 \text{ V}$ (dotted lines).

of the $\delta(\text{ND}_2)$ modes compared to the spectra measured in H_2O . Thus, in D_2O , in the base stacking spectral region, the carbonyl $\nu(\text{C}=\text{O})$ and in plane ring $\nu(\text{CC})_{\text{ip}}$ and $\nu(\text{C}=\text{N})$ stretching modes were present.^[14a,23] In addition, carrying out experiments in D_2O may affect the kinetics of chemical and biochemical processes.^[24] Indeed, our results showed that the aging of the $(\text{dCdG})_{20-65\%}$ DNA fragments was about half as fast in D_2O compared to H_2O (S2). The aging experiments were monitored using ex situ PM IRRAS. First, the $(\text{dCdG})_{20-65\%}$ SAMs were stored in either pure H_2O or in 10 mM PBS in H_2O . In H_2O , the first spectral changes, pointing to changes in the strength of hydrogen bonds between the base pairs, were observed in 3- to 4-day-old monolayers,^[14a] whereas in D_2O as the solvent, these effects were observable in 5-day-old monolayers (S2). The dsDNA aging process in the presence of ectoine was significantly slower in D_2O compared to H_2O solution. For this reason, experiments that were performed in D_2O were carried out for four weeks.

In the applied potential range, $-0.4 < E < 0.3$ V, even in a fresh dsDNA monolayer, no spectral changes were observed. It indicates that changes of the electric potential applied to the Au electrode had little effect on the stability and orientation of the DNA fragment containing four bases. In this potential range, alkanethiol monolayers are stable and cannot be electrochemically desorbed from the metal surface. To study a long-time effect of dsDNA interaction with ectoine, this narrow (700 mV) potential range was chosen. It is well documented in the literature that electric potentials affect the orientation of the helix axis.^[6a,b,7] The exact tilt of the dsDNA helix axis depends on the applied potential, surface concentration, and nucleic acid base composition of a DNA fragment in the monolayer. The orientation of DNA duplexes containing only two compatible nucleic acid bases seems to be more sensitive to electric potentials than of the fragments containing four bases. The negative electric potentials are responsible for an almost vertical orientation of the helix axis with respect to the substrate surface (monolayer plane). They lead to a relative reorientation of compatible bases, destabilizing the hydrogen bonds between them and finally to melting of the dsDNA. However, these potentials are more negative than the -0.4 V applied in this study.^[6b] Thus, in the studied $(\text{dCdG})_{20-65\%}$ DNA fragment, containing four bases, the applied potential range stabilized the preferential vertical to the monolayer surface double helix orientation.

Figure 3 displays multiple, overlapping IR absorption modes that underwent large spectral changes over time. In a 3-day-old monolayer, weak IR absorption modes were observed between 1700 and 1500 cm^{-1} (Figure 3b). In 21- and 28-day-old monolayers stored in 0.1 M ectoine solution, the intensities of the absorption modes in this spectral region increased. A new absorption mode appeared in the spectra at above 1700 cm^{-1} (Figure 3c, d). In addition, the in situ spectra differed from a calculated spectrum, which was determined from isotropic optical constants (S3) for a monolayer film consisting of randomly distributed $(\text{dCdG})_{20-65\%}$ DNA fragments in a helical A conformation (Figure 3a). Thus, changes in the shape and intensities of the IR spectra in the base stacking spectral region

featured a very complex pattern of DNA rearrangements in the monolayer film.

The number and position of the IR absorption modes, which contribute to the base stacking frequency region, reflect the strength of hydrogen bonds between the $\text{C}=\text{O}$ and the NH_2 (ND_2) groups and provide information about the DNA hybridization state.^[16b] To better interpret this information, spectra shown in Figure 3 were deconvoluted. Second-derivative and Fourier self-deconvolution (FSD) procedures were used to deconvolute these overlapping IR absorption modes. Figure 4 shows an example of the spectral deconvolution for random distribution of the $(\text{dCdG})_{20-65\%}$ fragment in a monolayer thick film. The deconvolution of this crowded spectral region is summarized in Table 1. In the base stacking frequency region, the $\nu(\text{C}=\text{O})$ modes are of great analytical significance, because their positions directly reflect the strength of the hydrogen bonds between two compatible bases. Below, the $\nu(\text{C}=\text{O})$ modes are analyzed in detail.

In the $(\text{dCdG})_{20-65\%}$ fragment, dAdT and dCdG base pairs contributed to the $\nu(\text{C}=\text{O})$ mode. In D_2O , in the dAdT base pair, T gives the $\nu(\text{C}=\text{O})_{\text{T}_2}$ around 1700 cm^{-1} and the $\nu(\text{C}=\text{O})_{\text{T}_4}$ between 1662 cm^{-1} and 1655 cm^{-1} .^[6a,14a,23a] In the random spectrum, the mode at 1703 cm^{-1} was assigned to the $\nu(\text{C}=\text{O})_{\text{T}_2}$ and the mode at 1660 cm^{-1} to the $\nu(\text{C}=\text{O})_{\text{T}_4}$ (Figure 4, Table 1). The dCdG base pair gave the $\nu(\text{C}=\text{O})$ modes around 1685 cm^{-1} to 1660 cm^{-1} , and 1663 cm^{-1} to 1640 cm^{-1} . The exact positions

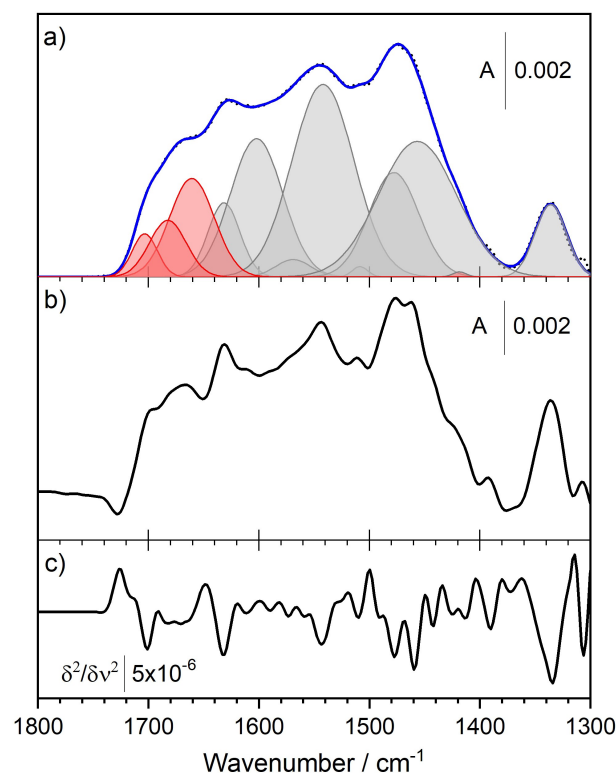


Figure 4. a) Deconvoluted calculated PM IRRAS b) Fourier self-deconvolution and c) second-derivative spectra of the $(\text{dCdG})_{20-65\%}$ fragments in the 1800 to 1300 cm^{-1} spectral region in a monolayer thick film (5.1 nm) at a surface concentration of $\Gamma = 5.5 \times 10^{-12}$ mol cm^{-2} . The IR absorption modes assigned to the $\nu(\text{C}=\text{O})$ modes are marked in red.

Table 1. Position and assignment of the deconvoluted IR absorption modes in the base stacking and glycosidic linkage spectral region of the (dCdG)₂₀₋₆₅% DNA fragment in a monolayer on the Au surface.

Wavenumber of the IR absorption mode/[cm ⁻¹]				Band assignment	Ref.
random	3-d-old PBS	21-d-old PBS + ectoine	28-d-old PBS + ectoine		
–	–	1744	1744	$\nu(\text{C}=\text{O})$ in T	[23a]
–	–	1725	1727	$\nu(\text{C}=\text{O})$ in G and C	[23a]
1703	–	1707	1701	$\nu(\text{C}=\text{O})_{\text{T}_2}$ in dAdT + $\nu(\text{C}=\text{O})$ in dCdG disrupted structure	
			1694		
1682	1686	1687	1680	$\nu(\text{C}=\text{O})$ in dCdG	
1660	1669	1663	1664	$\nu(\text{C}=\text{O})_{\text{T}_4}$ in dAdT + $\nu(\text{C}=\text{O})$ in dCdG	
	1647	1645	1644		
1631	1621	1627	1624	$\nu(\text{CC})_{\text{ip}}$ + $\nu(\text{C}=\text{N})$ in T and C	
1602	–	–	–	$\nu(\text{CC})_{\text{ip}}$ + $\nu(\text{C}=\text{N})$ in A	
1569	1580	1582	1580	$\nu(\text{CC})_{\text{ip}}$ + $\nu(\text{C}=\text{N})$ in A and G	
	1560	1559	1558		
1542	1536	1530	1535	$\nu(\text{CC})_{\text{ip}}$ + $\nu(\text{C}=\text{N})$ + $\delta(\text{CH})_{\text{ip}}$	
1509	1504	1498	–	$\delta(\text{ND}_2)$ + $\delta(\text{ND})_{\text{ip}}$ + $\delta(\text{CH})_{\text{ip}}$	[20a]
1478	1456	1462	1461	$\delta(\text{ND}_2)$ + $\delta(\text{ND})_{\text{ip}}$ + $\delta(\text{CH})_{\text{ip}}$	
1457	1436	1440	1440	$\delta(\text{ND}_2)$	

of these modes depended on the hydration and strength of hydrogen bonds between the bases C and G.^[6a,23a,25] The random spectrum of the (dCdG)₂₀₋₆₅% fragment gave the $\nu(\text{C}=\text{O})$ modes at 1682 cm⁻¹ and 1660 cm⁻¹, which were assigned to the dCdG base pairs (Table 1).

Compared to the random spectrum, in the 3-day-old (fresh) (dCdG)₂₀₋₆₅% SAM, some absorption modes disappeared, while others appeared in the in situ spectra (Figure 5 and Table 1). The strong dynamics of spectral changes indicated variations in the strength of hydrogen bonds between the bases, and thus possibly also of the hybridization state of the (dCdG)₂₀₋₆₅% DNA fragments. In the 3-day-old (dCdG)₂₀₋₆₅% SAM (stored in 10 mM PBS in D₂O) the IR absorption modes in this spectral region are about half as strong as in the random spectrum. Deconvolution gave three IR $\nu(\text{C}=\text{O})$ modes (Figure 5a, Table 1). The positions of the $\nu(\text{C}=\text{O})$ modes were characteristic for hydrogen bonded base pairs. Thus, the double helix structure of the (dCdG)₂₀₋₆₅% DNA fragment was confirmed. However, the $\nu(\text{C}=\text{O})_{\text{T}_2}$ mode was not visible in the PM IRR spectra (Figure 5a, Table 1). Indeed, in the (dAdT)₂₅ duplex monolayer on Au, the $\nu(\text{C}=\text{O})_{\text{T}_2}$ mode was also absent in the PM IRR spectra.^[6a] This is a consequence of the orientation of the double strand helix in the monolayer film and will be discussed below.

A few days of storage of the (dCdG)₂₀₋₆₅% SAM in 0.1 M ectoine D₂O solution caused no spectral changes (S2). Thus, in the presence of the compatible solute, the double helix structure of the (dCdG)₂₀₋₆₅% fragment was very stable. To elucidate the effect of ectoine on the stability and orientation of the double helix, in situ experiments were first conducted on 21- and 28-day-old (dCdG)₂₀₋₆₅% monolayers. In the $\nu(\text{C}=\text{O})$ stretching modes region, compared to fresh monolayers, the number of deconvoluted modes increased. This result indicates substantial changes in the network of hydrogen bonds within the (dCdG)₂₀₋₆₅% fragment. New IR absorption modes at 1744 cm⁻¹ and 1725 cm⁻¹ were detected (Figure 5b, c, Table 1). These IR absorption modes are characteristic for free, non-hydrogen bonded carbonyl groups, which can be attributed to

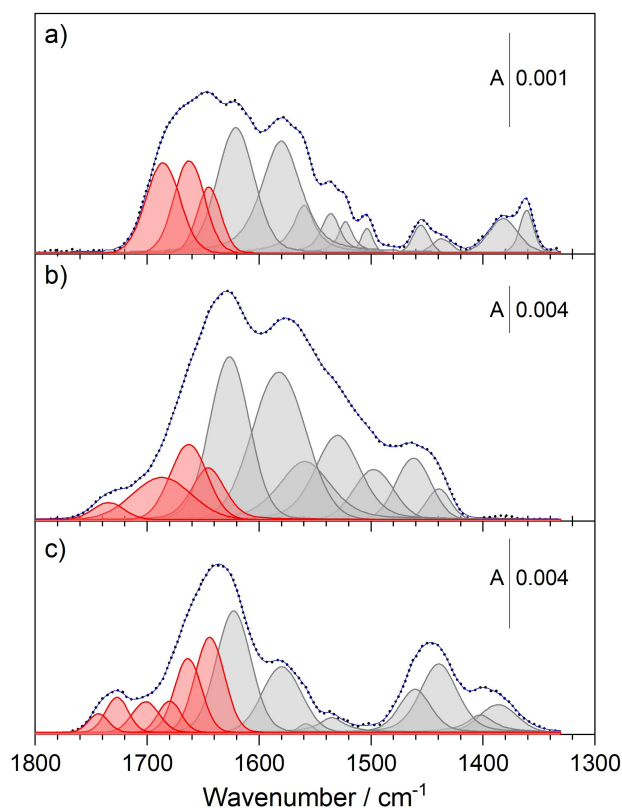


Figure 5. Deconvoluted PM IRR spectra in the 1800 cm⁻¹ to 1300 cm⁻¹ spectral region of a) 3-day-old (dCdG)₂₀₋₆₅% SAM stored in 10 mM PBS, D₂O b) 21- and c) 28-day old (dCdG)₂₀₋₆₅% SAMs stored in 0.1 M ectoine solution in D₂O; Electrolyte solution 10 mM PBS in D₂O at E = 0.0 V; The IR absorption modes assigned to the $\nu(\text{C}=\text{O})$ mode are marked in red.

the bases T, C, and G.^[23a,25] However, the $\nu(\text{C}=\text{O})$ modes found in fresh monolayers (at 1707, 1687, 1663, and 1645 cm⁻¹) were also found in PM IRR spectra of 21- and 28-day old monolayers, indicating that the ds(dCdG)₂₀₋₆₅% was still present in the monolayer film. In the PM IRR spectrum of a 28-day-old SAM a new band appeared at 1694 cm⁻¹. This mode was assigned to the dCdG base pair with weakened hydrogen

bonds.^[23a] In the base pair region, the DNA aging process was expressed as changes in the strength of the hydrogen bonds between base pairs, leading to a partial loss of hydrogen bonds between them, and thus a partial disruption of the helix structure. The presence of ectoine in the electrolyte solution slowed down the aging process. The appearance of IR signals from free nucleic acid bases indicates that some (dCdG)₂₀₋₆₅ % fragments lost the double helix structure, or even underwent dehybridization to a ssDNA. However, the presence of IR absorption modes characteristic for hydrogen bond base pairs indicates that some of the (dCdG)₂₀₋₆₅ % fragments retained their double helix structure, possibly partially disrupted.

Figures 5 and S2 show that not only the shape and number of the IR absorption modes but also their intensities changed over time. In a 3-day-old monolayer, the intensities of the IR absorption modes in the base stacking region were significantly lower compared to the random spectrum (Figures 4, 5, note the difference in scale between Figures). In contrast, in 21- and 28-day-old monolayers, these modes were more intense than in the random spectrum. These spectral changes arose from reorientations of the nucleic acid base pairs and thus of the long helix axis in the (dCdG)₂₀₋₆₅ % fragments as a function of time.^[6a] PM IRRAS is sensitive to the orientation of a molecule in an anisotropic film.^[6a,26] The integral intensity of a given IR absorption mode is proportional to the surface concentration of the adsorbed species (*I*) and the square of the absolute value of the dot product of the transition dipole moment vector changes during the normal vibration $\vec{\mu}'$ and the electric field vector of the p-polarized light \vec{E} :^[27]

$$I = \int Adv \cong \Gamma |\vec{\mu}'|^2 \langle \vec{E} \rangle^2 \cos^2 \theta \quad (2)$$

where θ is the angle between the $\vec{\mu}'$ and \vec{E} vectors. In PM IRRAS, the \vec{E} vector of the p-polarized light is oriented normal to the mirror (electrode) surface, thus changes in the integral intensity of a given IR absorption mode reflect reorientations of the $\vec{\mu}'$ vector with respect to the surface normal.

In a monolayer assembly, the dsDNA fragments have a similar spatial alignment, indicating that in the (dCdG)₂₀₋₆₅ % monolayer the $\vec{\mu}'$ vector of a given normal vibration [here $\nu(\text{C}=\text{O})$ modes] has a well-defined orientation. Figure 6 illustrates the relationship for differently oriented dsDNA fragments in a monolayer film.

The transition dipole moment vector of the $\nu(\text{C}=\text{O})$ modes lies along the carbonyl bonds, and thus in the plane of the aromatic rings of purine and pyrimidine.^[25] The transition dipole vectors of the ring stretching modes have different orientations with respect to the direction of the transition dipole moment of the $\nu(\text{C}=\text{O})$ modes, but they are also located in the ring plane. Therefore, the same pattern of spectral changes is expected, and indeed was observed, for all base stacking modes (Figure 4 and Figure 5). The integral intensities of IR absorption modes contributing to the $\nu(\text{C}=\text{O})$ modes in the (dCdG)₂₀₋₆₅ % SAM interacting with ectoine and for random distribution of the DNA fragment in the monolayer film were determined. We calculated the average tilt of the $\nu(\text{C}=\text{O})$ bonds in the (dCdG)₂₀₋₆₅ % SAMs, providing the average tilt of nucleic acid planes in the DNA

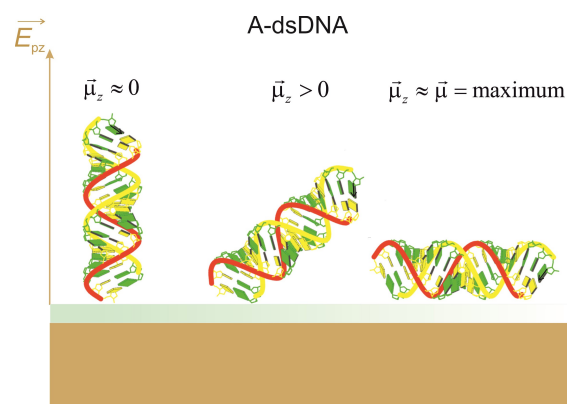


Figure 6. Cartoon showing different orientations of dsDNA fragments in the helical A conformation adsorbed to an Au surface via thiol linkage. The long axis of the A dsDNA is tilted by 0°, 45°, and 90° with respect to the surface normal. The orange arrow shows the direction of the electric field vector and the black arrows indicate orientations of the transition dipole vectors of $\nu(\text{C}=\text{O})$ and ring-stretching modes in nucleic acid bases.

fragment. However, within the C, G, and T planes the $\nu(\text{C}=\text{O})$ modes have different orientations.^[25] A possibility to determine the exact orientation of each $\nu(\text{C}=\text{O})$ mode would provide conclusions about the rotation of the aromatic ring plane in different nucleic acid bases. Below, we analyze the average orientation of the carbonyl group in nucleic acid bases in the (dCdG)₂₀₋₆₅ % fragment. In the 3-day-old (dCdG)₂₀₋₆₅ % SAM, the calculated average tilt of the $\nu(\text{C}=\text{O})$ bonds is $\theta_{(\nu(\text{C}=\text{O}))} = 68^\circ$ to the surface normal. In A-DNA, the plane of the parallel oriented base pairs made an angle of 70° with respect to the long helix axis.^[16b] This result indicates that the helix axis in (dCdG)₂₀₋₆₅ % is almost vertically oriented with respect to the surface normal. Indeed, in fresh dsDNA monolayers, a preferential orientation of the helical axis perpendicular to the Au surface was reported.^[3b,6a,7-8,28] With elapsing time, the ability of ectoine to bind water led to dehydration of the phosphate groups and stabilization of the A conformation, in particular in DNA fragments rich in dCdG base pairs.^[14a] The integral intensities of the $\nu(\text{C}=\text{O})$ increased and became stronger than in the random spectrum. In the 21-day-old (dCdG)₂₀₋₆₅ % monolayer, $\theta_{(\nu(\text{C}=\text{O}))}$ equaled 17° , and in the 28-day-old monolayer -42° . Considering that in these aged SAMs with interrupted helices the average inclination between the ring planes is the same as in A-DNA (close to 70°), the average inclination of the helical axis was calculated. It is in the range of 80° to 50° to the surface normal. Thus, over time the (dCdG)₂₀₋₆₅ % helices significantly changed their average orientation. This result is in line with the observed increase in the intensity of the $\nu_{as}(\text{PO}_2^-)$ mode (Figure 2). The transition dipole vector of the $\nu_{as}(\text{PO}_2^-)$ mode lies in the line connecting the two O atoms in the phosphate backbone. In the A conformation of dsDNA, the O...O line in the phosphate backbone has a preferential perpendicular orientation to the helix axis.^[16b] The transition dipole vector of the $\nu_s(\text{PO}_2^-)$ mode is perpendicular to the transition dipole vector of the $\nu_{as}(\text{PO}_2^-)$ mode and lies in the bisector of the OPO bonds. Tilting of the helix over time was consistent with an increase in the intensity of the $\nu_{as}(\text{PO}_2^-)$

mode and a decrease in the intensity of the $\nu_s(\text{PO}_2^-)$ mode. Thus, upon interaction with ectoine, the $(\text{dCdG})_{20-65\%}$ fragments gained some orientational flexibility. On the one hand, this flexibility may arise from dehybridization of double-stranded to single stranded DNA. On the other hand, a local breakdown of some hydrogen bonds between base pairs may lead to a local disruption of the double helix structure, without, however, a dissociation to ssDNA.

2.4. Hybridization of the dsDNA Monolayers Interacting with Ectoine

To further investigate the stability of the $(\text{dCdG})_{20-65\%}$ double helix in the monolayer film during interaction with ectoine, exonuclease VII (ExoVII) was used. Single stranded DNA is the substrate for this enzyme. During the enzymatic reaction, the hydrolysis of the ester bond joining phosphate and the ribose bond at the 5' and the 3' ends take place, leading to the formation of oligonucleosides.^[29] However, particularly in a short ssDNA fragment, mono- and di-nucleotides may also be formed. ExoVII is used as a specific marker for ssDNA. Thus, ExoVII would only be able to react with dehybridized $(\text{dCdG})_{20-65\%}$ terminal fragments. First, the affinity of ExoVII to a pure SC_6OH and $(\text{dCdG})_{20-65\%}$ SAMs was tested. Figure 7 shows PM IRRA spectra of the corresponding monolayers in the base stacking and glycosidic linkage spectral regions. The dotted line in Figure 7 shows that ExoVII adsorbed on the SC_6OH monolayer surface gave rise to an asymmetric amide I mode at 1660 cm^{-1} and the amide II mode at 1544 cm^{-1} . The amide I mode of ExoVII was deconvoluted (S4) into three modes centered at 1636 , 1660 and 1678 cm^{-1} . The amide I mode at 1636 cm^{-1} was assigned to β -sheets, at 1660 cm^{-1} to α -helices and at 1678 cm^{-1} to β -turns and loops. ExoVII is an asymmetric

protein composed of two subunits: XseA and XseB.^[30] These two subunits contain an OB-fold and catalytic domains, which are composed of a β -sheet, α -helices, and loop fragments, followed by a large α -helical domain and a C-terminal extension domain. All structural elements of the native ExoVII enzyme were confirmed when adsorbed on the SC_6OH monolayer.

In the $(\text{dCdG})_{20-65\%}$ SAM, the spectral changes confirmed the progress of the enzymatic reaction (Figure 7). For ExoVII attached to the $(\text{dCdG})_{20-65\%}$ SAM, the intensity of the broad IR absorption mode at 1700 cm^{-1} to 1600 cm^{-1} increased over time. With elapsing time, the shape of this mode changed and resembled the amide I mode of ExoVII adsorbed to the SC_6OH monolayer. Simultaneously, the intensity of the amide II increased, indicating the enzyme adsorption to the $(\text{dCdG})_{20-65\%}$ monolayer. Already in a 2-day-old monolayer a new IR absorption mode at $\sim 1710\text{ cm}^{-1}$, which arose from the $\nu(\text{C}=\text{O})$ in nucleic acid bases that were non-hydrogen bonded, was clearly visible in the spectra. It indicates the loss of the double helical structure in some of the $(\text{dCdG})_{20-65\%}$ fragments. A disruption of the double helix structure at the terminal $(\text{dCdG})_{20-65\%}$ fragment made it a substrate for ExoVII. After 6 days of ExoVII exposure to the $(\text{dCdG})_{20-65\%}$ SAM, the IR absorption modes in the base pair stacking and glycosidic linkage regions decreased in intensity. In contrast, storage of the monolayer in H_2O for 6 days led to a large increase in intensities of the IR absorption modes in this spectral region (S2). Thus, aging of the $(\text{dCdG})_{20-65\%}$ in the monolayer film is indeed accompanied by a partial dehybridization of double helices to ssDNA, which is proven by removal of nucleosides (oligonucleosides) by the enzyme and decrease in the intensities of the IR absorption modes in Figure 7. To elucidate the influence of ectoine on the interaction of ExoVII protein with dsDNA, a $(\text{dCdG})_{20-65\%}$ monolayer was incubated with ExoVII and buffer containing 2.5 M ectoine. This high concentration of ectoine corresponds to its biological concentration and thus was used to follow the enzymatic reaction. Furthermore, a $(\text{dCdG})_{20-65\%}$ monolayer was pre-incubated with 2.5 M ectoine buffer for 1 h, followed by an incubation with ExoVII in buffer without ectoine. Figure 8 shows the corresponding PM IRRA spectra.

Incubation of the $(\text{dCdG})_{20-65\%}$ monolayer in the buffer solution containing both ectoine (2.5 M) and ExoVII resulted in spectral changes that could be assigned to the adsorption of the enzyme to the monolayer surface. Thus, ectoine interaction with the $(\text{dCdG})_{20-65\%}$ DNA fragments did not affect the affinity of the enzyme to the monolayer.

The $\nu(\text{C}=\text{O})$ mode at $\sim 1720\text{ cm}^{-1}$, characteristic for free non-hydrogen bonded nucleic acid bases, was very weak. It indicated that predominantly nucleic acid base pairs were present in the monolayer. Thus, the $(\text{dCdG})_{20-65\%}$ fragment had a double helix structure. Over time, the intensity of the IR absorption modes in the base stacking region increased, which was due to ExoVII adsorption and gradual tilting of the helix axis toward the monolayer plane. No spectral evidence for the loss of the dsDNA structure was found (Figure 8a). However, pre-incubation of the $(\text{dCdG})_{20-65\%}$ SAM in 2.5 M ectoine solution for 1 h and subsequent immersion in the buffer

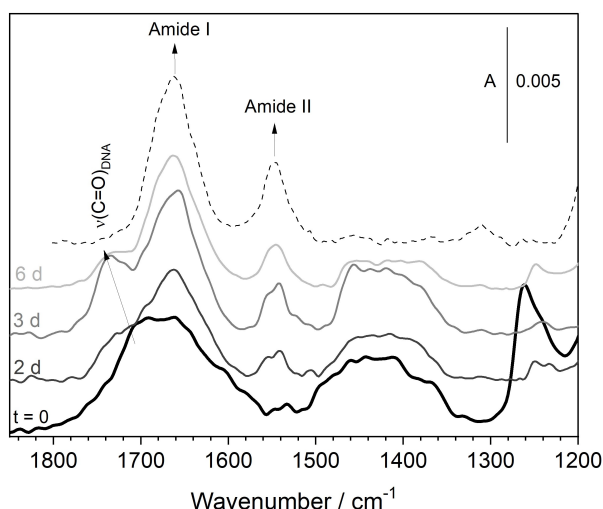


Figure 7. Ex situ PM IRRA spectra in the 1850 to 1300 cm^{-1} spectral region of the pure SC_6OH (dotted line) after 3 days of interaction with exonuclease VII and $(\text{dCdG})_{20-65\%}$ SAMs stored in 10 U exonuclease VII in H_2O interacting with the enzyme for 0 minutes (black line), 2, 3 and 6 days (grey lines, time marked in the figure).

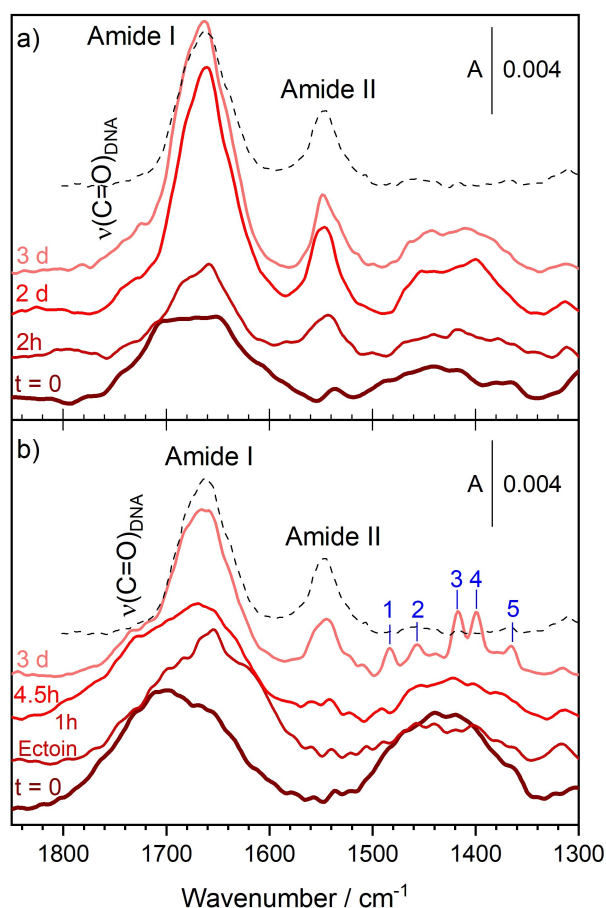


Figure 8. Ex situ PM IRRA spectra in the 1850 to 1300 cm^{-1} spectral region of the pure SC_6OH (dotted line) after 3 days of interaction with 10 U exonuclease VII and $(\text{dCdG})_{20-65\%}$ SAMs a) stored in 10 U enzyme solution with 2.5 M ectoine b) pre-incubated in 2.5 M ectoine solution for 1 h and then incubated in 10 U enzyme solution for different times marked in the Figure.

solution containing ExoVII showed different spectral characteristics. Already after 4.5 h incubation of the monolayer with ExoVII, an increase in the intensity at 1720 cm^{-1} was observed. After 3 days of interaction, the $\nu(\text{C}=\text{O})$ mode at $\sim 1720 \text{ cm}^{-1}$ appeared as a shoulder in the broad amide I of the enzyme and base-stacking mode. In the glycosidic linkage spectral region, large changes were observed (Figure 8b). A broad IR absorption mode, which is characteristic for dsDNA, became well resolved and composed of sharp signals centered at 1484, 1457, 1439, 1416, 1397, and 1364 cm^{-1} characteristic for nucleotides (numbered 1 to 5 in Figure 8).^[31] The resolution of individual IR absorption modes indicated that dehybridized DNA fragments were enzymatically hydrolyzed to short nucleotides. The base stacking region overlapped with the amide I mode, thus IR absorption modes from individual bases could not be identified. In summary, in the presence of ectoine, the enzymatic reaction was slow, indicating that the compatible solute hinders the enzymatic attack on the phosphate groups in DNA. This observation is consistent with published results.^[32] Ectoine is known to interact with phosphate O atoms in the phosphate-ribose backbone.^[14a,15] The ester-phosphate bond is hydrolyzed

by ExoVII.^[29b] In addition, ectoine is known to interact with proteins.^[33] Reducing the hydration shell of DNA by ectoine changes B to A dsDNA and may prevent the specific binding and proper orientation of the active center in ExoVII with respect to the substrate (ssDNA fragment), and thus hinder the progress of the enzymatic reaction.^[32] However, the presence of ectoine did not affect the adsorption of ExoVII onto the $(\text{dCdG})_{20-65\%}$ surface.

3. Conclusions

This work describes a holistic study of a dsDNA interaction with ectoine. Electrochemical studies demonstrated that the $(\text{dCdG})_{20-65\%}$ backfilled with a SC_6OH monolayer, when stored in aqueous solution, was stable up to 4 weeks. The stability of the monolayer made it possible to investigate the effect of time and of ectoine on the dsDNA hybridization state, its conformation, and orientation. Spectroelectrochemical results showed that electric potentials (at $-0.4 < E < 0.3 \text{ V}$) have little effect on the capacitance, hybridization, and orientation of the $(\text{dCdG})_{20-65\%}$ fragment in the monolayer film. In the $(\text{dCdG})_{20-65\%}$ SAM stored in PBS, no changes in the monolayer capacitance were observed. However, exposure of the $(\text{dCdG})_{20-65\%}$ monolayer to PBS solution containing ectoine led to a small increase in the monolayer capacitance. The sequence of spectral changes indicated that the interaction with ectoine involved dehydration of the phosphate groups, which stabilized the A conformation. Change in the DNA conformation caused by the dehydration of the phosphate-ribose backbone resulted in some reorientations of the base pairs. In turn, these reorientations let to a breakdown of hydrogen bonds between some base pairs and thus to a local disruption of the double helix structure. Accordingly, the $(\text{dCdG})_{20-65\%}$ fragment gained some orientational mobility. Over time, the orientation of the long axis of the double helix changed from vertical to the monolayer surface, which is characteristic for freshly made films,^[6a,7] to tilted.

Enzymatic studies with ExoVII indicated that the double helix structure of the $(\text{dCdG})_{20-65\%}$ fragment was preserved in the monolayer film immersed in ectoine solution.^[14a] Despite the fact that in some sections of the DNA fragment, hydrogen bonds between base pairs were broken, overall, the $\text{ds}(\text{dCdG})_{20-65\%}$, and not ssDNA fragments, were present in the monolayer. Ectoine is known to change the DNA conformation and, partially, the hybridization state.^[14a,15] Our results show that the enzymatic reaction of ExoVII was hindered in the presence of ectoine. It arose from the fact that both ectoine and ExoVII interact with the phosphate-ribose backbone. The presence of ectoine prevented the binding of the enzyme to the substrate. Our results demonstrate that in monolayer films, the addition of compatible solutes, such as ectoine, to the electrolyte solution may have a protective effect on dsDNA stability over time. This approach is attractive for the fabrication and storage of dsDNA devices such as biosensors.

Experimental Section

Materials and Chemicals

DNA sequences were synthesized by Metabion Int, AG (Martinsried, Germany): 5'- ACT TCG TGC GGC GCA TGC TG-(Thiol-C6)-3' (DNA) and 5'- CAG CAT GCG CCG CAC GAA GT -3' (DNA). Thiol-modified, single stranded ssDNA had a C₆-disulfide $-(\text{CH}_2)_6\text{S}-\text{S}-(\text{CH}_2)_6\text{-OH}$ modification at the 3'-end and formed (dCdG)₂₀-65% DNA duplexes with their unmodified complementary DNAs. 6-mercapto-1-hexanol (further abbreviated as: SC₆OH) was purchased from Sigma-Aldrich (Steinheim, Germany), Ectoine from AppliChem (AppliChem GmbH, Germany), and exonuclease VII (Cat. No. M0379L) from NewEngland Biolabs (Massachusetts, USA).

Microscope glass slides (VWR International, Darmstadt, Germany) were cut into 1.0×2.5 cm² pieces and rinsed with water (ELGA LabWater, Celle, Germany, conductivity ≤ 0.061 μS/cm) and ethanol (Fisher scientific UK, England, 99.99%). They were then dried in a stream of argon. On the cleaned glass surface, 0.5 nm of adhesive Cr and 150 nm Au (fine gold, Karl Fischer GmbH, Pforzheim, Germany) layers were evaporated using a Tectra MinoCoater (Tectra GmbH, Frankfurt/Main, Germany).

Preparation of dsDNA Monolayers on the Polycrystalline Gold Surface

Before each self-assembly, the gold substrates were rinsed with water and ethanol, dried with Ar and placed in an UV/ozone cleaner (Bioforce Nanoscience Inc., Ames, USA) for 10 min. First, the ssDNA fragments were diluted in water to yield 100 μM solutions. For the hybridization reaction, 100 μL of the reaction mixture containing 50 μL of a 10 mM K₂HPO₄/KH₂PO₄ phosphate buffer solution (PBS; K₂HPO₄ from Sigma-Aldrich, Japan, KH₂PO₄ from Sigma-Aldrich, USA) with 0.15 M NaCl (VWR Prolabo Chemicals, Belgium) and 0.1 M MgCl₂ (Sigma-Aldrich, China), 30 μL of thiol-modified DNA, and 20 μL of the compatible, unmodified DNA was prepared and left for 1 h to react. Prior to modification, the dsDNA sample was treated with tris(2-carboxyethyl)phosphine hydrochloride (TCEP, Sigma-Aldrich, Switzerland) for 1 h for disulfide-bond reduction. Next, a few drops of the solution were placed on the surface of a gold slide. For DNA immobilization, the electrode was covered with a lid and left for approximately 18 h for self-assembly at room temperature. On the next day, the dsDNA-modified electrode was rinsed with 10 mM PBS, pH 7 and exposed to a 2 mM (SC₆OH) solution in 10 mM PBS for 30 min (backfilling). Subsequently, the dsDNA – SC₆OH monolayer on the gold surface was again rinsed with 10 mM PBS, pH 7, and used in further experiments.

Interaction of dsDNA Monolayers with Ectoine

As a control experiment to confirm that self-assembly of the monolayer was successful, PM IRRAS spectra of freshly prepared dsDNA monolayers were first recorded. Next, the gold slide covered with the dsDNA monolayer was immersed either in water or in 10 mM phosphate buffer with 0.1 M ectoine solution in either H₂O or D₂O. The samples were stored in these solutions for up to 4 weeks, during which the PM IRRAS spectra of the monolayer samples were measured.

Interaction of dsDNA Monolayers with Exonuclease VII

The gold slide covered with the dsDNA monolayer was treated with 10 U of the Exonuclease VII, ExoVII, (Cat. No. M0379L) in the provided enzyme reaction buffer (10 mM Tris-HCl, 10 mM sodium

phosphate, 1.6 mM EDTA, 2 mM 2-mercaptoethanol, pH 8) either alone or additionally in the presence of 2.5 M ectoine. The samples were incubated for different times at 37 °C, during which the PM IRRAS spectra of the monolayer samples were measured.

Electrochemical Measurements

Electrochemical measurements were performed in an all-glass, three-electrode cell using an evaporated polycrystalline Au electrode (area 0.22 cm²) as the working electrode (WE). A gold wire was used as a counter electrode (CE), and an Ag|AgCl|sat.KCl (Ag|AgCl) as a reference electrode (RE). A Methrom Autolab potentiostat (Utrecht, Netherlands) was used to perform the electrochemical measurements. Before the experiment, the cell was purged with argon for 30 minutes. The electrochemical cell's cleanliness was tested by recording electrical potential – capacitance plots of the polycrystalline Au electrode in 10 mM PBS in H₂O (pH 7.2). Next, Au WE with a self-assembled (dCdG)₂₀-65% monolayer was immersed in the PBS or PBS with 0.1 M ectoine electrolyte solution. Alternating current voltammograms of the WE were recorded at amplitude of 10 mV, and a frequency of 20 Hz at a scan rate of 5 mVs⁻¹. Software versions Nova v.2.1 and v.2.1.3 were used to analyze the electrochemical results.

In situ PM IRRAS Measurements

The PM IRRAS spectra were recorded using a Vertex 70 spectrometer with a photo-elastic modulator ($f=50$ kHz; PMA 50, Bruker, Ettlingen, Germany) and demodulator (Hinds Instruments, OR, USA). A home-made spectroelectrochemical glass cell was washed in water, then in ethanol, and dried in an oven at 60 °C. After rinsing the CaF₂ prism with water and ethanol, it was cleaned using a UV ozone chamber (Bioforce Nanosciences, VA, USA) for 10 minutes. The spectroelectrochemical cell has a built-in platinum CE. The RE was Ag|AgCl in 3 M KCl in either D₂O or H₂O. A disc polycrystalline gold electrode (dia. 15 mm, Alfaeser, Karlsruhe, Germany) was used as WE and as a mirror for the IR radiation. The Au electrode was covered by (dCdG)₂₀-65% monolayer. First, the in situ spectra of a freshly adsorbed (dCdG)₂₀-65% monolayer were measured (electrolyte solution 10 mM PBS, H₂O) as well as the spectra of a monolayer stored in 10 mM PBS in D₂O for 3 days (electrolyte solution 10 mM PBS, D₂O). The monolayer was further stored in 0.1 M ectoine solution in D₂O and measured after 21 and 28 days of storage. Additionally, the (dCdG)₂₀-65% monolayer was stored in 0.1 M ectoine solution in H₂O and in situ spectra were measured after 7 and 14 days of storage.

In situ experiments, the electrolyte solution was 10 mM PBS in H₂O or D₂O. The difference between pH and pD is ca. 0.3.^[34] The electrolyte solution was purged for 1 hour with argon to remove oxygen. At each potential applied to the Au electrode, 400 spectra with a resolution of 4 cm⁻¹ were measured. The spectra were recorded at half-wave retardation set to 1600 cm⁻¹ and the angle of incidence of the incoming IR radiation was 55°. The thickness of the electrolyte layer between the CaF₂ prism and Au electrode varied between 4 and 6 μm. In each experiment, 7–14 potential scans at 0.3, 0.1, 0, -0.1, -0.2, -0.3, and -0.4 V in the negative- and positive-going potential scans were recorded. The analysis of PM IRRAS spectra was carried out using OPUS v5.5 software (Bruker, Ettlingen, Germany).

Ex situ PM IRRAS Measurements

PM IRRAS spectra at the gold|air interface were recorded at an angle of incidence of the IR light $\varphi=80^\circ$ to surface normal. The half-wave

retardation was set to 1600 cm⁻¹ and the spectrometer resolution to 4 cm⁻¹. In each experiment 400–600 PM IRRA spectra were recorded. These spectra were recorded to check the self-assembly process of the (dCdG)_{20-65%} monolayer and to follow the progress of the (dCdG)_{20-65%} monolayer interaction with Exo VII. Raw PM IRRA spectra were background-corrected using the OPUS V5.5 program (Bruker, Ettlingen, Germany).

Acknowledgements

Open access funding enabled and organized by Projekt DEAL.

Conflict of Interest

The authors declare no conflict of interest.

Keywords: DNA · self-assembled monolayer · ectoine · in situ spectroelectrochemistry · enzymatic reaction

- [1] a) E. Palecek, M. Bartosik, *Chem. Rev.* **2012**, *112*, 3427–3481; b) R. L. Zaffino, T. Galan, W. A. Pardo, M. Mir, J. Samiter, *Wiley Interdiscip. Rev. Nanomed. Nanobiotechnol.* **2015**, *7*, 817–827.
- [2] a) H. Sun, Y. Qiu, Y. Lu, J. Kong, X. Zhang, *Chem. Commun.* **2020**, *56*, 6636–6639; b) E. E. Ferapontova, *Chem. Asian J.* **2019**, *14*, 3773–3781; c) M. Gebala, W. Schumann, *Phys. Chem. Chem. Phys.* **2012**, *14*, 14933–14942; d) A. Verhaven, T. Doneux, D. Bizzotto, *Langmuir* **2018**, *34*, 14802–14810.
- [3] a) A. B. Steel, T. M. Herne, M. J. Tarlov, *Anal. Chem. (Wash.)* **1998**, *70*, 4670–4677; b) U. Rant, K. Arinaga, S. Fujita, N. Yokoyama, G. Abstreiter, M. Tornow, *Org. Biomol. Chem.* **2006**, *4*, 3448–3455.
- [4] L. Kekedy-Nagy, E. E. Ferapontova, *Angew. Chem. Int. Ed.* **2019**, *58*, 3048–3052; *Angew. Chem.* **2019**, *131*, 3080–3084.
- [5] S. Mahajan, J. Richardsan, T. Brown, P. N. Bartlett, *J. Am. Chem. Soc.* **2008**, *130*, 15589–15601.
- [6] a) L. Kekedy-Nagy, E. E. Ferapontova, I. Brand, *J. Phys. Chem. C* **2017**, *121*, 1552–1565; b) R. P. Johnson, N. Gale, J. A. Richardson, T. Brown, P. N. Bartlett, *Chem. Sci.* **2013**, *4*, 1625; c) A. W. Peterson, R. J. Heaton, R. M. Georgiadis, *Nucleic Acids Res.* **2001**, *29*, 5163–5168; d) I. Y. Wong, N. A. Melosh, *Nano Lett.* **2009**, *9*, 3521–3526.
- [7] S. O. Kelley, J. K. Barton, N. M. Jackson, L. D. McPherson, A. B. Potter, E. M. Spain, M. J. Allen, M. G. Hill, *Langmuir* **1998**, *14*, 6781–6784.
- [8] U. Rant, K. Arinaga, S. Fujita, N. Yokoyama, G. Abstreiter, M. Tornow, *Nano Lett.* **2004**, *4*, 2441–2445.
- [9] R. Campos, A. Kotlyar, E. E. Ferapontova, *Langmuir* **2014**, *30*, 11853–11857.
- [10] I. Kocsis, A. Rotaru, Y. M. Legrand, I. Grosu, M. Barboiu, *Chem. Commun.* **2016**, *52*, 386–389.
- [11] a) P. H. Yancey, *J. Exp. Biol.* **2005**, *208*, 2819–2830; b) B. Kempf, E. Bremer, *Arch. Microbiol.* **1998**, *170*, 319–330; c) A. Ventosa, J. J. Nieto, A. Oren, *Microbiol. Mol. Biol. Rev.* **1998**, *62*, 504–544.
- [12] a) M. B. Hahn, T. Solomun, R. Wellhausen, S. Hermann, H. Seitz, S. Meyer, H. J. Kunte, J. Zeman, F. Uhlig, J. Smiatek, H. Sturm, *J. Phys. Chem. B* **2015**, *119*, 15212–15220; b) J. Smiatek, *J. Phys. Chem. B* **2014**, *118*, 771–782; c) J. Smiatek, R. K. Harishchandra, O. Rubner, H. J. Galla, A. Heuer, *Biophys. Chem.* **2012**, *160*, 62–68.
- [13] a) E. A. Oprzeska-Zingrebe, S. Meyer, A. Roloff, H. J. Kunte, J. Smiatek, *Phys. Chem. Chem. Phys.* **2018**, *20*, 25861–25874; b) E. A. Oprzeska-Zingrebe, M. Kohagen, J. Kaestner, J. Smiatek, *Eur. Phys. J.: Spec. Top.* **2019**, *227*, 1665–1679; c) S. Meyer, M. A. Schröter, M. B. Hahn, T. Solomun, H. Sturm, H. J. Kunte, *Sci. Rep.* **2017**, *7*, 7170; d) C. S. V. Rajendrakumar, T. Suryanarayana, A. R. Reddy, *FEBS Lett.* **1997**, *410*, 201–205.
- [14] a) J. Wittmar, S. Meyer, T. Sieling, J. Kunte, J. Smiatek, I. Brand, *J. Phys. Chem. B* **2020**, *124*, 7999–8011; b) P. W. Rakowska, M. Kogut, J. Czub, J. Stangret, *J. Mol. Liq.* **2018**, *271*, 186–201.
- [15] M. B. Hahn, G. J. Smales, H. Seitz, T. Solomon, H. Sturm, *Phys. Chem. Chem. Phys.* **2020**, *22*, 6984–6992.
- [16] a) D. R. Whelan, T. J. Hiscox, J. I. Rood, K. R. Bamberg, D. McNaughton, B. R. Wood, *J. R. Soc. Interface* **2014**, *11*, 20140454; b) B. R. Wood, *Chem. Soc. Rev.* **2016**, *45*, 1999–2018; c) S. Adam, J. Liquier, J. A. Taboury, E. Taillandier, *Biochemistry* **1986**, *25*, 3220–3225; d) R. Letellier, M. Ghomi, E. Taillandier, *J. Biomol. Struct. Dyn.* **1986**, *3*, 671–687; e) J. A. Taboury, J. Liquier, E. Taillandier, *Can. J. Chem.* **1985**, *63*, 1904–1909.
- [17] C. Vericat, M. E. Vela, G. Benitez, P. Carro, R. C. Salvezza, *Chem. Soc. Rev.* **2010**, *39*, 1805.
- [18] S. Flock, R. Labarbe, C. Houssier, *Biophys. J.* **1996**, *71*, 1519–1529.
- [19] J. Liquier, E. Taillandier, in *Infrared Spectroscopy of Biomolecules* (Eds.: H. H. Mantsch, D. Chapman), Wiley-Liss, New York, **1996**.
- [20] a) M. Tsuboi, *Appl. Spectrosc. Rev.* **1969**, *3*, 45–90; b) S. Adam, J. A. Taboury, E. Taillandier, A. Popinel, T. Huynh-Dinh, J. Igolen, *J. Biomol. Struct. Dyn.* **1985**, *3*, 873–885.
- [21] K. C. Lu, E. W. Prohofsky, L. L. van Zandt, *Biopolymers* **1977**, *16*, 2491–2506.
- [22] T. Shimanouchi, M. Tsuboi, Y. Kyogoku, *Infrared spectra of nucleic acids and related compounds, Vol. 7*, Interscience, New York, **1964**, pp 467–499.
- [23] a) C. Lee, M. Cho, *J. Chem. Phys.* **2006**, *125*, 114509/1–12; b) D. R. Whelan, K. R. Bamberg, P. Heraud, M. J. Tobin, M. Diem, D. McNaughton, B. R. Wood, *Nucleic Acids Res.* **2011**, *39*, 5439–5448.
- [24] a) S. Dongmo, G. Wittstock, J. Christoffers, I. Brand, *Electrochim. Acta* **2017**, *255*, 198–208; b) E. Pines, in *Isotope Effects In Chemistry and Biology* (Eds.: A. Kohen, H.-H. Limbach), CRC Press **2005**, pp. 451–464; c) O. Farver, J. Zhang, Q. Chi, I. Pecht, J. Ulstrup, *Proc. Natl. Acad. Sci. USA* **2001**, *98*, 4426–4430; d) J. D. E. McIntyre, M. Salomon, *Prepr. Pap. Am. Chem. Soc. Div. Fuel Chem.* **1967**, *11*, 209–217.
- [25] C. Lee, K. H. Park, M. Cho, *J. Chem. Phys.* **2006**, *125*, 114508/1–16.
- [26] I. Brand, Application of polarization modulation infrared reflection absorption spectroscopy in electrochemistry, Springer Nature, Cham, **2020**, pp 1–122.
- [27] a) D. L. Allara, R. G. Nuzzo, *Langmuir* **1985**, *1*, 52–66; b) V. Zamylny, J. Lipkowski, in *Advances in electrochemical science and engineering, Vol. 9* (Eds.: R. C. Alkire, D. M. Kolb, J. Lipkowski, P. N. Ross), Wiley-VCH, Weinheim, **2006**, pp. 315–376.
- [28] E. A. Josephs, T. Ye, *Nano Lett.* **2012**, *12*, 5255–5261.
- [29] a) J. W. Chase, C. C. Richardson, *J. Biol. Chem.* **1974**, *249*, 4545–4552; b) J. W. Chase, C. C. Richardson, *J. Biol. Chem.* **1974**, *249*, 4553–4561.
- [30] K. Poleszak, K. H. Kaminska, S. Dunin-Horkawicz, A. Lupas, K. J. Skowronek, J. M. Bujnicki, *Nucleic Acids Res.* **2012**, *40*, 8163–8174.
- [31] R. Santamaria, E. Charro, A. Zacarias, C. M., *J. Comput. Chem.* **1999**, *20*, 511–530.
- [32] G. Malin, R. Iakobashvili, A. Lapidot, *J. Biol. Chem.* **1999**, *274*, 6920–6929.
- [33] a) A. Roychoudhury, D. Haussinger, F. Oesterhelt, *Protein Pept. Lett.* **2012**, *19*, 791–794; b) I. Yu, Y. Jindo, M. Nagaoka, *J. Phys. Chem. B* **2007**, *111*, 10231–10238; c) I. Yu, M. Nagaoka, *Chem. Phys. Lett.* **2004**, *388*, 316–321.
- [34] F. G. K. Baucke, *J. Phys. Chem. B* **1998**, *102*, 4835–4841.

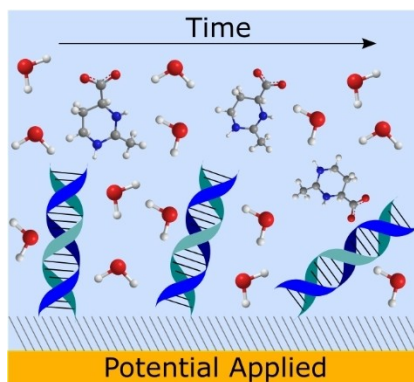
Manuscript received: June 14, 2021

Revised manuscript received: July 17, 2021

Accepted manuscript online: July 19, 2021

ARTICLES

Providing long term stability: In the presence of the compatible solute ectoine, dsDNA monolayer films preserve a double helix structure for four weeks. Electric potentials affect neither the conformation nor the structure of the DNA. A dehydration of the phosphate groups leads to a transition to the A conformation. This sequence of events is accompanied by a gradual tilting of the double helix and dehybridization to the single helix is not observed.



*J. Wittmar, Dr. C. Ohle, Dr. J. Kunte,
Dr. I. Brand**

1 – 12

Effect of Ectoine on the Conformation and Hybridization of dsDNA in Monolayer Films: A Spectroelectrochemical Study



Open Access